Applied Nanoscience (2023) 13:5477–5488
https://doi.org/10.1007/s13204-022-02735-9

ORIGINAL ARTICLE

Density functional theory and molecular docking study to lutein molecule for COVID-19 protease inhibitors

Dhaidan Khalaf Kafi[1] · **Adil N. Ayyash**[2]

Received: 25 August 2022 / Accepted: 9 December 2022 / Published online: 19 January 2023

Abstract

Since the beginning of the corona pandemic, numerous scientific projects have been conducted worldwide to investigate how the new virus can be combated. Researchers are developing various vaccines and drugs at full speed – with varying degrees of success. In this work, silico screening (molecular docking analysis) is performed on twenty natural compounds, which are expected to provide valuable lead molecules and medication to treat a new condition SARS-CoV-2. Our results indicate that out of the 20 compounds on the candidate list, lutein and Polydatin, natural components of fruits and vegetables (especially egg yolk and maize) have shown an excellent performance in our docking studies through a minimum binding energy of − 9.8 kcal/mol also − 7.4 kcal/mol, separately. This indicates their potential for the inhibitory molecular interactions against COVID-19. The main intent of the research is to analyse the protein components and investigate the molecules.

Keywords COVID-19 · Polyphenols · Molecular docking · Active sites.Lutein

Introduction

The corona pandemic has affected a big part of the world, with massive limitations on everyday life and unprecedented damage to society and Business (Donthu and Gustafsson 2020). Until the widespread use of the vaccines or a specific therapies can be implemented against the SARS-CoV-2 virus is available, compliance with the "AHAL rules" for effective infection prevention in social interaction is essential (AHAL: Keep your distance, observe hygiene measures, in everyday life wear a mask, make air in closed rooms) (P. Reich And A. Elward 2019; Abdelsattar et al. 2021; Gössling et al. 2020). Basically, a remedy is urgently needed and sought that will help to prevent or at least slow down viral infections and reduce the severity of the symptoms without provoking resistance. Not just against SARS-CoV-2, medical laboratories around the world are working flat out to develop a vaccine (Machhi et al. 2020). There cannot be a quick solution for this, because of the legal approval regulations. Combating viral infections also faced the problem of the rapid mutability of viruses. Vaccinations only help against strains that are already known, not against those that have already changed and developed resistance (PhilippeBuchy et al. 2020). For this, the scientist mixes empirical information from conventional medicine with big science data and intricate computer simulations to find additional promising therapeutic prospects (Hilbert 2016; Pham et al. 2020). The activation of Nrf2, which could be a potential victim to prevent and/or lessen the severity of SARS-CoV-2 infection, reduce oxidative stress and inflammation, boost innate immunity, and downregulate ACE2 receptors, is anticipated to occur when flavonoid additives are taken in conjunction with vitamin D3.

The research team has thus been successful in isolating plant compounds that are effective against both influenza viruses and pneumococci. Scientists will comb through hundreds of extracts from fungi, medicinal plants and microbes, over-the-counter remedies such as vitamins, trace elements and certain plant substances seem to be able to prevent COVID-19, as doctors observed in over hundreds of patients (Balboni et al. 2022). Polyphenols are aromatic compounds that contain two or more hydroxyl groups directly attached to the aromatic ring and are classified as secondary plant

✉ Dhaidan Khalaf Kafi
dhkh77@yahoo.com

Adil N. Ayyash
sc.adil_nameh78@uoanbar.edu.iq

[1] Department of Medical Physics, College of Applied Science, University of Fallujah, Baghdad, Iraq

[2] Department of Physics, College of Science, University of Anbar, Ramadi, Iraq

substances (Vuolo et al. 2019). Natural polyphenols are present in plants as bioactive components such flavorings, tannic acids, and colorants (flavonoids, anthocyanins) (tannins). Through their color, they are intended to deter predators from the plant or draw insects for pollination (Alihosseini 2016). The biochemical simulation suggests that the conclusions of the 17 components of garlic are a valuable, natural antiviral source that helps prevent the attack of the coronavirus into the human cells". This is published on April 2, 2020 by a team of researchers from various universities in Vietnam (Thuy et al. 2020). A scheduling and resource management solution that includes built-in time tracking, job management, Gantt charts, and invoicing.

Background study

Many polyphenols are considered beneficial to health. Plants with a high polyphenol content, for example, the aronia berry, the leaves and grapes of red vines are also known as red wine or sherry in particular the skin and the pulp of the mangostine tree fruit (Garcinamangostana) due to the high number of different molecular compounds of xanthones. The juice of the pomegranate (Punica granatum) contains among others, punicalagin, crosmine, ellagic acid and gallic acid, ginkgo, tea, rock rose, perilla seed (Perilla frutescens), black nettle, Chinese lemon balm, wild sesame (Costa et al. 2017; Cory et al. xxxx). More than 8000 phenolic structures are known. Their common feature is an aromatic ring bearing a hydroxy group (Croft 1998). Polyphenols can be divided into different subclasses based on their chemical structure (Watzl and Rechkemmer 2001)0.1- Flavonoids 2- phenolic acids and their derivatives (so-called "non-flavonoids")3-Chalcones. Polyphenols often have the ability to bind proteins and minerals and are therefore assigned to the group of vegetable tanning agents. The astringent effect when eating many fruits and drinks is due to the reaction of salivary proteins with plant polyphenol. Polyphenols have anti-inflammatory and cancer-preventive effects, among other things, Polyphenols have been shown in studies to stop the growth of cancer factions in the mammary glands, lungs, skin, intestines, and prostate(GiusiBriguglio et al. xxxx). Flavonoids and anthocyanins shield cells are from free radicals and slow cell oxidation. They prevent arteriosclerosis by reducing fat deposits (plaques) in the blood vessels. For example, after one year of using a pomegranate preparation, the depth of the inner wall of the carotid artery in patients with arteriosclerosis decreased by 30%, while it increased by 9% in the command group (Achraf et al. 2018). Furthermore, Vanderbilt University Medical Center was able to prove that regular fruit juice consumption can reduce the risk of Alzheimer's disease by up to 76%, for which polyphenols are also held responsible (Chai et al. 2019). At the same time, polyphenols from plant foods can bind to digestive enzymes and thus reduce nutrient absorption in the intestine. In healthy people, the proline-rich proteins contained in the saliva prevent this effect by forming a stable complex with the polyphenols in the digestive tract. Polyphenol inhibits the bacterial species Streptococcus mutants, which contributes to the build-up of dental plaque, and is therefore also a preventative against tooth (Cory et al. xxxx; Bimonte et al. 2019). A physiologically active polyphenol called epigallocatechin-3-galeate (EGCG) was isolated and extracted from Camellia Sinensis. It has in studies prevented virus infection, containing coronaviruses. In recent double-blind, placebo-controlled clinical trials, the incidence of respiratory infections among medical personnel during an H1N1 influenza outbreak was found to decrease by up to 75%, while improving systemic immunity by increasing T-cell proliferation (28%), and IFN- production (26%). In studies, the molecular docking studies against the coronavirus disease COVID-19, caused by SARS-CoV-2, has been identified as the source of the outbreak. EGCG has been discovered as a candidate with a very high potential for COVID-19 antiviral chemoprophylaxis. Most of the literature did not expose much about density functional theory and molecular docking studies. To determine the electronic structure of atoms, molecules, and solids, chemists and physicists employ the density functional theory (DFT) quantum–mechanical (QM) technique. Since the 1970s, it has gained a lot of traction in computational solid-state physics. The molecular docking method allows us to define how tiny molecules behave in the binding site of target proteins and to better understand basic biological processes by simulating the interaction between a small molecule and a protein at the atomic level. The primary objective of this study is to determine whether different polyphenol-containing compounds can prevent COVID-19, enhance systemic immunity, lower the rate of acute respiratory illness, and decrease the frequency and strength of designated symptoms of COVID-19. Moreover, the exploration of the results will help in selecting symptoms for COVID-19.

Computational methods

A computer emulation of a candidate for binding a ligand to a receptor is known as molecular docking. When two molecules are bound together to form a stable complex, the preferred orientation of one molecule to the other is predicted by this technique. The results of this technique can be utilized to estimate the power of association or binding attraction between the two molecules. In this situation, the molecular scoring function is also helpful. Molecular docking and computational discovery are of great benefit to the scientific community, offering a time- and cost-efficient way to assess the interaction between molecules. This is a

particularly useful tool for assessing how molecules might behave prior to their introduction into cultured cells or a living organism.

Typically, this method takes into account biologically significant substances such proteins, polypeptide, nucleic acids, carbohydrates, and fats. These molecules are extremely important and play an important role in our body's signaling mechanisms. As a result, the type of signal generated depends on the orientation of the two molecules that will interact during this signal transduction process. In other words, molecular docking is crucial for figuring out the type and strength of the signal produced during biological signaling.

Furthermore, molecular docking methods are critical in the development of construction-based drugs. This is because of the predictability of small molecules like phenols binding to an appropriate binding location. The main bioactive compounds of polyphenol natural compounds (see Table 1) were investigated using molecular docking program AutoDoc Vina (Huey et al. 2012) and in accordance with the Data from Hsu (2015) evaluated as potential ligands for the COVID-19 viral protein. The small molecules like water molecules were removed. Both protein and phenolic compound structures were improved using AutoDock Tool (ADT) (Huey et al. 2012). Charges, polar hydrogen atoms, and rotatable bonds were set using the MGLTools package (Tresanco et al. 2020). All of the atoms in the ligand set were included in the centergridbox's dimensions. By using a grid of 60, 60, and 60 points (for x, y, and z), the location of the grid box was determined to be at $x = -10.729$, $y = 12.417$, and $z = 68.816$. The replication of viruses and their attachment to host cells were the focus of this study. We chose the spike protein in COVID-19 as our target for the docking investigations as a result. The Protein Data Bank (PDB) code 6LU7used to retrieve the spike protein's structural information.

Table 1 The docking affinity and the RMSD lower and upper bound of the phenolic compounds against the COVID-19 spike protein

compound	mode	affinity	dist from best mode	
	#	(kcal/mol)	RMSD lower bound	RMSD upper bound
lutein	4	− 9.5	1.872	4.823
Polydatin	5	− 7.6	3.897	6.262
Quercetin	8	− 7.4	2.131	7.868
Luteolin	6	− 7.3	3.522	4.786
Kaempferol	2	− 7.3	2.653	7.574
Galangin	4	− 7.3	3.203	5.973
Eriodictyol	2	− 7.3	2.091	7.453
Naringenin	7	− 7.1	3.092	5.526
Apigenin	5	− 7.1	3.152	5.441
Genistein	5	− 7	1.359	7.615
Daidzein	8	− 6.8	3.276	6.405
Resveratrol	6	− 6.7	0.169	2.247
Chrysin	3	− 6.7	2.961	5.494
bcaroten	4	− 6.3	1.779	7.124
Rutein	5	− 5.7	2.697	9.314
Syringic_aci	1	− 5.3	0.871	3.43
Caffeic	8	− 5.2	0.807	2.045
acaroten	9	− 5.2	1.804	2.198
Lignin	6	− 5.7	0.894	3.743
ferulic acid	5	− 5.8	2.872	3.651

The structures of the phytochemicals utilized as ligands were downloaded as SDF files from the PubChem Compound database (https://pubchem.ncbi.nlm.nih.gov/). We picked 20 naturally occurring substances that contain polyphenols. To transform 2D structures into 3D ones and minimize computational mistakes, the OPLS3 force field was used. At most five isomers were produced for each ligand when ionization states were applied with Epik at pH 7.00 (Dilshad et al. 2022). To account for the flexibility of amino acid residues at the active binding site and prevent false-positive data from the bonding process, induced-fit docking (IFD) was selected (Dennington et al. 2009). Affinity binding (Kcal/mol) was used to define the output docking scores. The Discovery Studio version V20 was used to create the interactions between the ligands and proteins (Dilshad et al. 2022). The specified molecule's ground-state structure was calculated using DFT extracted in the B3LYP/6-311G** model. A frequent abbreviation used in quantum chemical calculations is B3LYP, which stands for Becke'sfunction for exchanging three parameters combined with Lee–Yang–Parr non-native correlation functional. The Gaussian 09 W program was used to do all calculations (Sherman et al. 2006). The optimized shape, HOMO–LUMO, and MEP as well as the assignments of the vibrational bands were visualized through the graphical tool Gauss View 6 (Studio 2008).

Results and discussions

Molecular docking studies of phenolic compounds

The results of the molecular docking are summarized in Table 1. It is clear that most phenolic compounds showed a good binding affinity against COVID-19. The docking binding affinity ranges between − 9.5 and 5.2 kcal/mol. The flavonol di-hexose such as lutein and Polydatin showed the highest binding affinity against COVID-19 and other phenolic compounds. The docking binding affinity for rutin and Polydatin is − 9.50 and − 7.4 kcal/mol, respectively. In contrast, the docking scores for flavone mono-hexose such as Caffeic and a carotene are − 5.2 kcal/mol. The Quercetin analogues showed lower binding energy than

lutein analogues. The docking binding affinity suggested most phenolic high binding affinity against COVID-19. Consequently, most likely they would bind and inhibit the virus.

The Root mean square deviation (RMSD) values measuring the average distance between atoms of a position relative to the best fitting position are calculated using only movable heavy atoms. Two variants of RMSD metrics are provided, rmsd/lb ((RMSD lower bound) and rmsd/ub (RMSD upper bound)), differing in how the atoms are matched in the distance calculation: rmsd/ub matches each atom in one conformation with itself in the other conformation, ignoring any symmetry. Rmsd' matches each atom in one conformation with the closest atom of the same element type in the other conformation rmsd/lb defined as follows: rmsd/lb (c1, c2) = max (rmsd' (c1, c2), rmsd' (c2, c1)), with cn conformation n.

The calculated RMSD/lb values vary between 3.2 and 1.9 A., whereas RMSD/ulb values are varying between 9.3 and 2.0 A. These results indicated that most of the phenolic compounds present some changes after binding to the virus. The values of the RMSD/lb and RMSD/ub of Rutin are 1.87 and 4.8, respectively. This indicated that the phenolic compounds lutein with the highest binding affinity to the virus did not encounter any destruction after binding to the virus.

Structural analysis of lutein

Figure 1 showed that the molecular structure that had been optimized. Table 2 displays a differentiation of particular adjusted geometric factors with experimental results (Sathish et al. xxxx). The calculated and experimental bond lengths accord well with one another. While the two aromatic rings C-C bond lengths are discovered to be in the range of 1.55, this result is because of the delocalization of electrons, the C-C bond lengths in the core chains C15-C21, C24-C28, C33-C34, C41-C42, C35-C36, C33-C32, C30-C27 at 1.35- 1.45 A correspondingly. The carbon-oxygen single bonds are C6-O1 (1.4617Å) and C13-O2 (1.4622 A). The C-C-C bond angles in the benzene ring are 110 to 120°, it is discovered that the result agrees with these values (Kafi et al. 1178). The bond angles of O-C-Chad been calculated at 106.2812to111.8634)Å. The calculated torsion angles of the compound show that the compound is not planar.

HOMO and LUMO Study

The frontier molecular orbitals (HOMO) and (LUMO) are essential for determining electric properties in theoretical chemistry. The conversion of HOMO orbitals to LUMO orbitals, where HOMO stands for electron donors and LUMO for electron acceptors, is reflected in the absorption of light (Kafi et al. 1178). Fig. 2 displays the planes of the boundary molecular orbitals for the aforementioned molecule. The HOMO and LUMO are evenly dispersed across the entire molecule, with the exception of hydrogen atoms in the HOMO orbital and H atoms and carbonyl oxygen in the LUMO orbital.LUMO densities are primarily found on the carbon atoms of the phenyl and phenol molecule as well as on the core chain's C–C single bond. Due to the many abundant electron groups of atomic orbitals, the HOMO to LUMO electronic transition is therefore predominantly found through theπ -π* electronic transitions. The computed HOMO and LUMO energies are − 4.43435 eV and − 2.201124 eV, respectively, while the compound's frontier orbital energy gap of 2.23323 eV.

Molecular electrostatic potential analysis

The relationship between the electronic arrangement and chemical reactivity of a compound can be determined particularly well using the molecular electrostatic potential (MEP). The MEP expresses a potential difference, i.e. a voltage difference between two places. This means that the energy is determined at a point in space, which experiences a test charge (positive unit charge) when brought from infinity

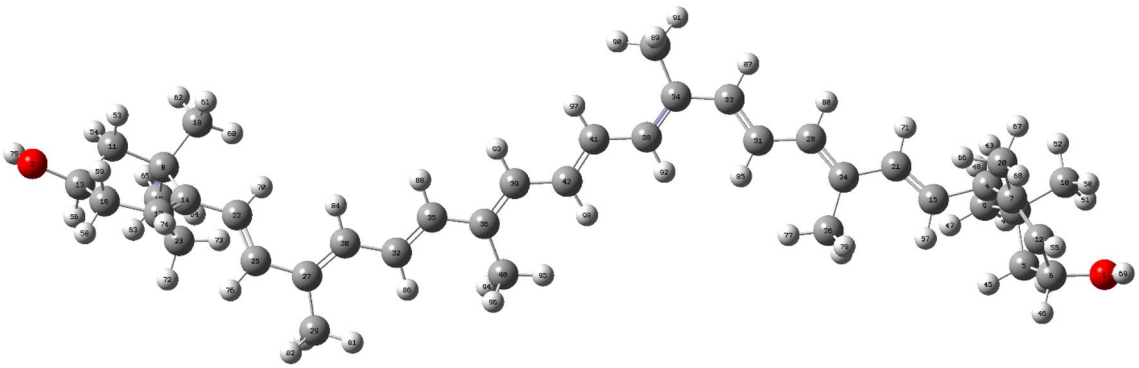

Fig. 1 The minimized structure of Lutein

Table 2 Bond (lengths, angles and dihedral angles) of Lutein

Bond Length		Bonds angles		Dihedral angle	
R(1,6)	1.4617	A(6,1,69)	109.5025	D(69,1,6,5)	167.0905
R(1,69)	0.9796	A(13,2,75)	109.7946	D(69,1,6,12)	43.0345
R(2,13)	1.4622	A(4,3,5)	110.9849	D(69,1,6,46)	− 76.2705
R(2,75)	0.9786	A(4,3,9)	110.529	D(75,2,13,11)	62.6742
R(3,4)	1.5537	A(4,3,10)	109.0392	D(75,2,13,16)	− 178.0454
R(3,5)	1.551	A(5,3,9)	109.0117	D(75,2,13,56)	− 59.6235
R(3,9)	1.5447	A(5,3,10)	111.1085	D(5,3,4,7)	49.2794
R(3,10)	1.5488	A(9,3,10)	108.1668	D(5,3,4,15)	− 74.2675
R(4,7)	1.5543	A(3,4,7)	111.642	D(5,3,4,43)	166.9895
R(4,15)	1.517	A(3,4,15)	114.181	D(9,3,4,7)	169.0606
R(4,43)	1.101	A(3,4,43)	107.0102	D(9,3,4,15)	45.5137
R(5,6)	1.5515	A(7,4,15)	108.5131	D(9,3,4,43)	− 73.2292
R(5,44)	1.0962	A(7,4,43)	107.7834	D(10,3,4,7)	− 72.1613
R(5,45)	1.0988	A(15,4,43)	107.4374	D(10,3,4,15)	164.2918
R(6,12)	1.5051	A(3,5,6)	114.6421	D(10,3,4,43)	45.5488
R(6,46)	1.1016	A(3,5,44)	109.9351	D(4,3,5,6)	− 55.4984
R(7,12)	1.3444	A(3,5,45)	108.8113	D(4,3,5,44)	− 177.1643
R(7,20)	1.5094	A(6,5,44)	107.8426	D(4,3,5,45)	66.1306
R(8,11)	1.5532	A(6,5,45)	108.4666	D(9,3,5,6)	− 176.2148
R(8,14)	1.5538	A(44,5,45)	106.8557	D(9,3,5,44)	62.1193
R(8,18)	1.5538	A(1,6,5)	106.6695	D(9,3,5,45)	− 54.5858
R(8,19)	1.554	A(1,6,12)	110.8678	D(10,3,5,6)	64.674
R(9,47)	1.0952	A(1,6,46)	107.1007	D(10,3,5,44)	− 56.9918
R(9,48)	1.0971	A(5,6,12)	113.5219	D(10,3,5,45)	− 173.697
R(9,49)	1.0969	A(5,6,46)	109.0375	D(4,3,9,47)	− 62.8345
R(10,50)	1.0915	A(12,6,46)	109.4137	D(4,3,9,48)	57.4545
R(10,51)	1.0959	A(4,7,12)	120.8188	D(4,3,9,49)	176.7886
R(10,52)	1.0979	A(4,7,20)	116.0534	D(5,3,9,47)	56.9305
R(11,13)	1.5552	A(12,7,20)	122.1006	D(5,3,9,48)	177.2196
R(11,53)	1.0985	A(11,8,14)	111.0964	D(5,3,9,49)	− 63.4463
R(11,54)	1.1	A(11,8,18)	107.0035	D(10,3,9,47)	177.8585
R(12,55)	1.0912	A(11,8,19)	110.005	D(10,3,9,48)	− 61.8524
R(13,16)	1.5196	A(14,8,18)	111.0376	D(10,3,9,49)	57.4817
R(13,56)	1.1005	A(14,8,19)	109.2482	D(4,3,10,50)	59.0895
R(14,17)	1.3634	A(18,8,19)	108.3942	D(4,3,10,51)	178.3659
R(14,22)	1.4749	A(3,9,47)	111.954	D(4,3,10,52)	− 62.4686
R(15,21)	1.3523	A(3,9,48)	110.9255	D(5,3,10,50)	− 61.0507
R(15,57)	1.0886	A(3,9,49)	110.0571	D(5,3,10,51)	58.2257
R(16,17)	1.5183	A(47,9,48)	107.6625	D(5,3,10,52)	177.3912
R(16,58)	1.0987	A(47,9,49)	108.201	D(9,3,10,50)	179.3331
R(16,59)	1.1016	A(48,9,49)	107.8996	D(9,3,10,51)	− 61.3905
R(17,23)	1.5139	A(3,10,50)	112.0906	D(9,3,10,52)	57.775
R(18,60)	1.0945	A(3,10,51)	110.1853	D(3,4,7,12)	− 25.3166
R(18,61)	1.0961	A(3,10,52)	110.1275	D(3,4,7,20)	156.5465
R(18,62)	1.097	A(50,10,51)	107.1892	D(15,4,7,12)	101.3813
R(19,63)	1.0956	A(50,10,52)	109.0212	D(15,4,7,20)	− 76.7556
R(19,64)	1.0953	A(51,10,52)	108.1033	D(43,4,7,12)	− 142.5609
R(19,65)	1.0976	A(8,11,13)	112.7417	D(43,4,7,20)	39.3022
R(20,66)	1.0974	A(8,11,53)	109.8434	D(3,4,15,21)	− 120.8009
R(20,67)	1.0992	A(8,11,54)	108.8175	D(3,4,15,57)	61.3813
R(20,68)	1.0947	A(13,11,53)	107.5487	D(7,4,15,21)	113.9807
R(21,24)	1.4602	A(13,11,54)	110.6587	D(7,4,15,57)	− 63.8372
R(21,71)	1.091	A(53,11,54)	107.0716	D(43,4,15,21)	− 2.3006
R(22,25)	1.3585	A(6,12,7)	120.9484	D(43,4,15,57)	179.8815

Table 2 (continued)

Bond Length		Bonds angles		Dihedral angle	
R(1,6)	1.4617	A(6,1,69)	109.5025	D(69,1,6,5)	167.0905
R(22,70)	1.0882	A(6,12,55)	115.8729	D(3,5,6,1)	− 88.2136
R(23,72)	1.0998	A(7,12,55)	119.1669	D(3,5,6,12)	34.1894
R(23,73)	1.0913	A(2,13,11)	111.8634	D(3,5,6,46)	156.4435
R(23,74)	1.099	A(2,13,16)	106.2812	D(44,5,6,1)	34.5878
R(24,26)	1.5115	A(2,13,56)	109.2694	D(44,5,6,12)	156.9907
R(24,28)	1.3714	A(11,13,16)	109.3479	D(44,5,6,46)	− 80.7551
R(25,27)	1.4652	A(11,13,56)	110.1947	D(45,5,6,1)	149.9693
R(25,76)	1.0893	A(16,13,56)	109.8012	D(45,5,6,12)	− 87.6278
R(26,77)	1.0911	A(8,14,17)	122.1996	D(45,5,6,46)	34.6264
R(26,78)	1.098	A(8,14,22)	114.8738	D(1,6,12,7)	112.9268
R(26,79)	1.0981	A(17,14,22)	122.9245	D(1,6,12,55)	− 65.8043
R(27,29)	1.5158	A(4,15,21)	124.266	D(5,6,12,7)	− 7.1221
R(27,30)	1.3705	A(4,15,57)	115.7198	D(5,6,12,55)	174.1468
R(28,31)	1.4368	A(21,15,57)	119.9784	D(46,6,12,7)	− 129.1676
R(28,80)	1.0909	A(13,16,17)	113.5276	D(46,6,12,55)	52.1013
R(29,81)	1.0923	A(13,16,58)	109.8625	D(4,7,12,6)	3.3039
R(29,82)	1.0976	A(13,16,59)	107.8144	D(4,7,12,55)	− 178.0036
R(29,83)	1.0992	A(17,16,58)	109.5826	D(20,7,12,6)	− 178.672
R(30,32)	1.4375	A(17,16,59)	110.0894	D(20,7,12,55)	0.0205
R(30,84)	1.0895	A(58,16,59)	105.6553	D(4,7,20,66)	54.19
R(31,33)	1.3672	A(14,17,16)	122.8815	D(4,7,20,67)	− 64.2078
R(31,85)	1.0868	A(14,17,23)	124.6535	D(4,7,20,68)	175.2548
R(32,35)	1.3682	A(16,17,23)	112.425	D(12,7,20,66)	− 123.9412
R(32,86)	1.0864	A(8,18,60)	112.2927	D(12,7,20,67)	117.661
R(33,34)	1.4541	A(8,18,61)	111.0373	D(12,7,20,68)	− 2.8764
R(33,87)	1.0908	A(8,18,62)	109.5237	D(14,8,11,13)	− 42.687
R(34,37)	1.5174	A(60,18,61)	108.5351	D(14,8,11,53)	77.2361
R(34,38)	1.3757	A(60,18,62)	107.2667	D(14,8,11,54)	− 165.847
R(35,36)	1.4456	A(61,18,62)	108.0253	D(18,8,11,13)	− 164.0416
R(35,88)	1.0906	A(8,19,63)	111.4785	D(18,8,11,53)	− 44.1185
R(36,39)	1.3782	A(8,19,64)	110.6757	D(18,8,11,54)	72.7984
R(36,40)	1.5133	A(8,19,65)	110.4772	D(19,8,11,13)	78.41
R(37,89)	1.0993	A(63,19,64)	107.5655	D(19,8,11,53)	− 161.6669
R(37,90)	1.0926	A(63,19,65)	108.3104	D(19,8,11,54)	− 44.75
R(37,91)	1.0964	A(64,19,65)	108.2125	D(11,8,14,17)	9.6208
R(38,41)	1.4309	A(7,20,66)	110.993	D(11,8,14,22)	− 170.8969
R(38,92)	1.0894	A(7,20,67)	110.737	D(18,8,14,17)	128.5812
R(39,42)	1.43	A(7,20,68)	111.7884	D(18,8,14,22)	− 51.9364
R(39,93)	1.0908	A(66,20,67)	106.7626	D(19,8,14,17)	− 111.9198
R(40,94)	1.0977	A(66,20,68)	108.3224	D(19,8,14,22)	67.5625
R(40,95)	1.091	A(67,20,68)	108.0477	D(11,8,18,60)	− 169.5187
R(40,96)	1.0978	A(15,21,24)	126.7036	D(11,8,18,61)	68.7604
R(41,42)	1.3728	A(15,21,71)	118.0296	D(11,8,18,62)	− 50.4578
R(41,97)	1.0884	A(24,21,71)	115.2668	D(14,8,18,60)	69.0895
R(42,98)	1.0883	A(14,22,25)	126.127	D(14,8,18,61)	− 52.6314
R(73,76)	2.4766	A(14,22,70)	116.2728	D(14,8,18,62)	− 171.8496
		A(25,22,70)	117.4913	D(19,8,18,60)	− 50.9186
		A(17,23,72)	111.6339	D(19,8,18,61)	− 172.6395
		A(17,23,73)	112.8058	D(19,8,18,62)	68.1423
		A(17,23,74)	109.5423	D(11,8,19,63)	− 59.5112
		A(72,23,73)	107.813	D(11,8,19,64)	− 179.1899
		A(72,23,74)	106.2666	D(11,8,19,65)	60.9742
		A(73,23,74)	108.5227	D(14,8,19,63)	62.6876

Table 2 (continued)

Bond Length		Bonds angles		Dihedral angle	
R(1,6)	1.4617	A(6,1,69)	109.5025	D(69,1,6,5)	167.0905
		A(21,24,26)	118.0268	D(14,8,19,64)	− 56.9912
		A(21,24,28)	118.4241	D(14,8,19,65)	− 176.8271
		A(26,24,28)	123.5491	D(18,8,19,63)	− 176.1928
		A(22,25,27)	126.6628	D(18,8,19,64)	64.1284
		A(22,25,76)	118.0547	D(18,8,19,65)	− 55.7074
		A(27,25,76)	115.2276	D(8,11,13,2)	179.6583
		A(24,26,77)	112.7065	D(8,11,13,16)	62.2031
		A(24,26,78)	110.8476	D(8,11,13,56)	− 58.5745
		A(24,26,79)	110.8647	D(53,11,13,2)	58.421
		A(77,26,78)	107.667	D(53,11,13,16)	− 59.0342
		A(77,26,79)	107.6494	D(53,11,13,56)	− 179.8118
		A(78,26,79)	106.8527	D(54,11,13,2)	− 58.2129
		A(25,27,29)	115.1816	D(54,11,13,16)	− 175.6681
		A(25,27,30)	121.7098	D(54,11,13,56)	63.5542
		A(29,27,30)	123.1081	D(2,13,16,17)	− 167.867
		A(24,28,31)	128.1419	D(2,13,16,58)	69.0426
		A(24,28,80)	116.7019	D(2,13,16,59)	− 45.6313
		A(31,28,80)	115.1559	D(11,13,16,17)	− 46.9545
		A(27,29,81)	112.999	D(11,13,16,58)	− 170.0449
		A(27,29,82)	110.3858	D(11,13,16,59)	75.2811
		A(27,29,83)	111.1942	D(56,13,16,17)	74.0624
		A(81,29,82)	107.5553	D(56,13,16,58)	− 49.028
		A(81,29,83)	107.787	D(56,13,16,59)	− 163.7019
		A(82,29,83)	106.6407	D(8,14,17,16)	4.0487
		A(27,30,32)	127.4178	D(8,14,17,23)	− 173.4745
		A(27,30,84)	117.2711	D(22,14,17,16)	− 175.3918
		A(32,30,84)	115.3035	D(22,14,17,23)	7.0849
		A(28,31,33)	122.948	D(8,14,22,25)	− 135.7115
		A(28,31,85)	118.0954	D(8,14,22,70)	40.3793
		A(33,31,85)	118.9479	D(17,14,22,25)	43.7666
		A(30,32,35)	123.1357	D(17,14,22,70)	− 140.1426
		A(30,32,86)	117.9806	D(4,15,21,24)	− 178.4058
		A(35,32,86)	118.8826	D(4,15,21,71)	1.6444
		A(31,33,34)	127.9507	D(57,15,21,24)	− 0.6755
		A(31,33,87)	116.8932	D(57,15,21,71)	179.3748
		A(34,33,87)	115.1411	D(13,16,17,14)	15.288
		A(33,34,37)	115.4497	D(13,16,17,23)	− 166.9159
		A(33,34,38)	122.3208	D(58,16,17,14)	138.5319
		A(37,34,38)	122.2288	D(58,16,17,23)	− 43.6721
		A(32,35,36)	126.6018	D(59,16,17,14)	− 105.6778
		A(32,35,88)	117.6911	D(59,16,17,23)	72.1183
		A(36,35,88)	115.7071	D(14,17,23,72)	− 106.4155
		A(35,36,39)	118.5534	D(14,17,23,73)	15.17
		A(35,36,40)	118.3942	D(14,17,23,74)	136.1632
		A(39,36,40)	123.0523	D(16,17,23,72)	75.8345
		A(34,37,89)	111.2483	D(16,17,23,73)	− 162.58
		A(34,37,90)	112.7826	D(16,17,23,74)	− 41.5869
		A(34,37,91)	110.5095	D(15,21,24,26)	− 0.0361
		A(89,37,90)	107.6689	D(15,21,24,28)	179.9371
		A(89,37,91)	106.8279	D(71,21,24,26)	179.9148
		A(90,37,91)	107.5399	D(71,21,24,28)	− 0.1119
		A(34,38,41)	127.1815	D(14,22,25,27)	− 178.6514
		A(34,38,92)	117.5955	D(14,22,25,76)	4.1822

Table 2 (continued)

Bond Length		Bonds angles		Dihedral angle	
R(1,6)	1.4617	A(6,1,69)	109.5025	D(69,1,6,5)	167.0905
		A(41,38,92)	115.2212	D(70,22,25,27)	5.3002
		A(36,39,42)	128.1832	D(70,22,25,76)	− 171.8661
		A(36,39,93)	116.5047	D(17,23,73,76)	− 65.918
		A(42,39,93)	115.3119	D(72,23,73,76)	57.8055
		A(36,40,94)	110.8464	D(74,23,73,76)	172.5099
		A(36,40,95)	112.615	D(21,24,26,77)	− 179.5701
		A(36,40,96)	110.9082	D(21,24,26,78)	− 58.8144
		A(94,40,95)	107.5685	D(21,24,26,79)	59.6846
		A(94,40,96)	107.0053	D(28,24,26,77)	0.4581
		A(95,40,96)	107.6534	D(28,24,26,78)	121.2139
		A(38,41,42)	123.7534	D(28,24,26,79)	− 120.2872
		A(38,41,97)	118.4593	D(21,24,28,31)	− 179.6465
		A(42,41,97)	117.7844	D(21,24,28,80)	0.1475
		A(39,42,41)	123.6425	D(26,24,28,31)	0.3252
		A(39,42,98)	118.6614	D(26,24,28,80)	− 179.8809
		A(41,42,98)	117.6952	D(22,25,27,29)	− 155.0325
		A(23,73,76)	94.7812	D(22,25,27,30)	25.222
		A(25,76,73)	83.5991	D(76,25,27,29)	22.2032
				D(76,25,27,30)	− 157.5423
				D(22,25,76,73)	− 64.9328
				D(27,25,76,73)	117.5797
				D(25,27,29,81)	− 163.4715
				D(25,27,29,82)	− 42.9873
				D(25,27,29,83)	75.1615
				D(30,27,29,81)	16.2701
				D(30,27,29,82)	136.7542
				D(30,27,29,83)	− 105.097
				D(25,27,30,32)	− 177.1365
				D(25,27,30,84)	3.9234
				D(29,27,30,32)	3.1384
				D(29,27,30,84)	− 175.8016
				D(24,28,31,33)	179.1022
				D(24,28,31,85)	0.1892
				D(80,28,31,33)	− 0.6944
				D(80,28,31,85)	− 179.6074
				D(27,30,32,35)	− 178.8708
				D(27,30,32,86)	1.5099
				D(84,30,32,35)	0.0871
				D(84,30,32,86)	− 179.5322
				D(28,31,33,34)	179.1671
				D(28,31,33,87)	− 2.317
				D(85,31,33,34)	− 1.9287
				D(85,31,33,87)	176.5872
				D(30,32,35,36)	179.8378
				D(30,32,35,88)	− 0.1369
				D(86,32,35,36)	− 0.5462
				D(86,32,35,88)	179.4791
				D(31,33,34,37)	164.5415
				D(31,33,34,38)	− 15.1654
				D(87,33,34,37)	− 13.9964
				D(87,33,34,38)	166.2967
				D(33,34,37,89)	− 82.219
				D(33,34,37,90)	156.6814

Table 2 (continued)

Bond Length		Bonds angles		Dihedral angle	
R(1,6)	1.4617	A(6,1,69)	109.5025	D(69,1,6,5)	167.0905
				D(33,34,37,91)	36.2766
				D(38,34,37,89)	97.4882
				D(38,34,37,90)	− 23.6114
				D(38,34,37,91)	− 144.0161
				D(33,34,38,41)	176.9661
				D(33,34,38,92)	− 3.5627
				D(37,34,38,41)	− 2.721
				D(37,34,38,92)	176.7501
				D(32,35,36,39)	179.9457
				D(32,35,36,40)	− 0.181
				D(88,35,36,39)	− 0.0791
				D(88,35,36,40)	179.7943
				D(35,36,39,42)	179.4422
				D(35,36,39,93)	− 0.3967
				D(40,36,39,42)	− 0.4249
				D(40,36,39,93)	179.7363
				D(35,36,40,94)	59.2335
				D(35,36,40,95)	179.7987
				D(35,36,40,96)	− 59.4832
				D(39,36,40,94)	− 120.8992
				D(39,36,40,95)	− 0.334
				D(39,36,40,96)	120.3841
				D(34,38,41,42)	179.0272
				D(34,38,41,97)	− 1.6013
				D(92,38,41,42)	− 0.4547
				D(92,38,41,97)	178.9168
				D(36,39,42,41)	179.98
				D(36,39,42,98)	− 0.3579
				D(93,39,42,41)	− 0.1795
				D(93,39,42,98)	179.4826
				D(38,41,42,39)	179.4137
				D(38,41,42,98)	− 0.2514
				D(97,41,42,39)	0.0382
				D(97,41,42,98)	− 179.6269
				D(23,73,76,25)	130.6576

to this point. Or more vividly, it is determined by how "comfortable" this positive charge feels at this point. The MEP is calculated at this location in a simplified manner by summing the interaction of all charges in the molecule with this test charge. The MEP expresses energy, which corresponds to a voltage difference (in volts). However, the specification in kilocalories per mole or kilojoules per mole is more widespread. For the coloring of the molecules, the MEP was calculated for all points on a molecule surface and these were colored accordingly (Deghady et al. 2021; Chen et al. 2016; Islam et al. 2021; Das et al. xxxx). The color scale extends from red to blue. Red areas represent areas with a strongly negative MEP (excess of electrons), i.e. areas in which positive charges feel “comfortable”. In blue areas, the MEP is positive and there is an electron deficit and the positive charges are “uncomfortable” here, but negative charges are “very exultant” there. These results are in agreement with the results of the close compound vanillin in the structure (Le et al. 2020; Sathish et al. xxxx).

In the case of Lutin, it is clear that the red color is the dominant. Therefore, rutin has a high activity towards different chemical compound. This may explain the high affinity towards the COVID-19 spike protein.

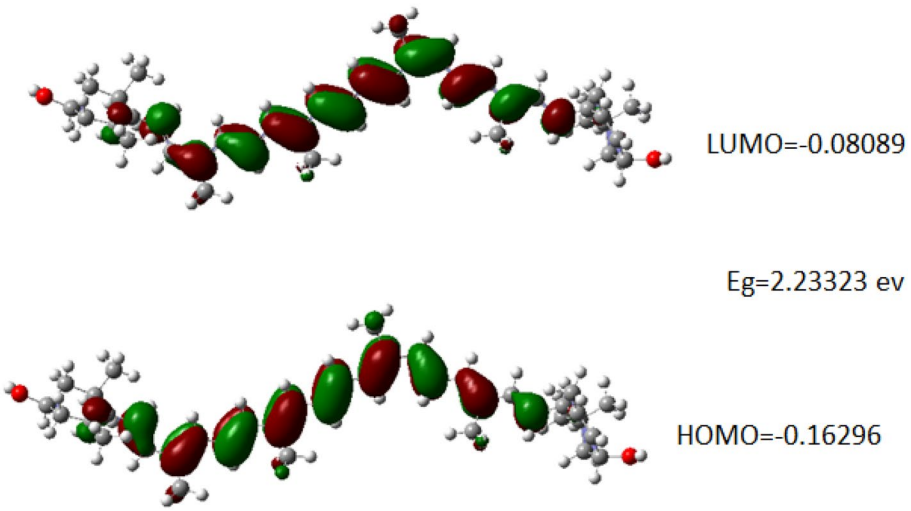

Fig. 2 Frontier molecular orbitals of the investigated molecule

Docking analysis of Rutin with the s-pike protein

To gain better insight into the type of interactions between phenolic compounds and the spike protein of the COVID-19 virus, we investigated the binding interactions of Lutin against the virus to understand its inhibitory mechanism. Figure 3 shows the main interaction between the rutin and the protein. It is clear that the binding interactions of Lutin-versus and the protein had cooperative sharing interactions. It has hydrogen bonding with UnK0 residue. Moreover, the aromatic rings of flavonoids and phenolic acids generate π-sigma interaction with His 41 and alkyl with Met94. Fig. 4. shows ligand interaction between rutin against S-protein in COVID-19 virus. The H-bond, π-sigma and alkyle interactions are shown as green, blue lavender dotted lines, respectively (Shelley et al. 2007; Chen et al. 2016). Figs 5 and 6 present the 3D and 2D interaction between the Lutein and the active sites of the protein. It is clear that the results suggest the strong affinity of Lutin with the protein by the common amino acid Met and HIS. Numerous studies confirm our conclusions (Sathish et al. xxxx; Islam et al.2021; Das et al. xxxx).

It is believed that the polyphenols in the extract prevent viruses from docking and penetrating into the host cell through interactions with the viral surface antigens. This would be a new antiviral principle of action, because the antivirals commonly used today, such as Lutin, only attack the virus when the replication cycle is advanced by inhibiting the release of the already multiplied viruses or virus particles from the host cell.

Whether certain polyphenols of the mentioned extract are responsible for the effect has not yet been clarified. In any case, it is much more effective than other (sometimes completely ineffective) rutin or Polydatin from green leafy vegetables such as spinach, which are also typical polyphenol drugs.

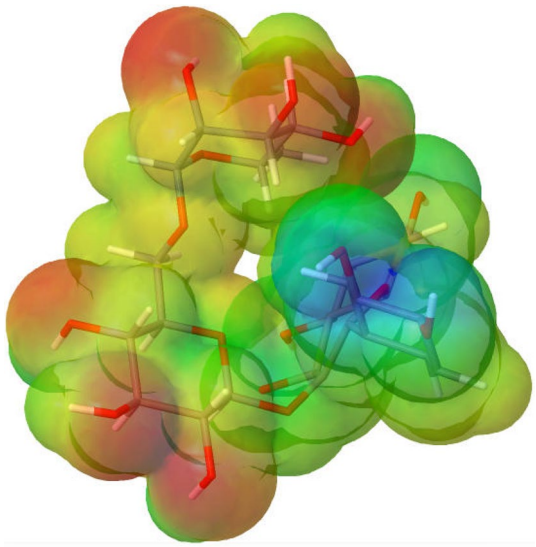

Fig. 3 Molecular electrostatic potential Map of Lutin

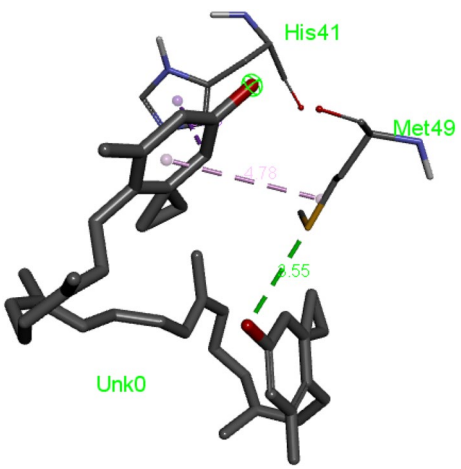

Fig. 4 Ligands interactions between Lutin against S-protein

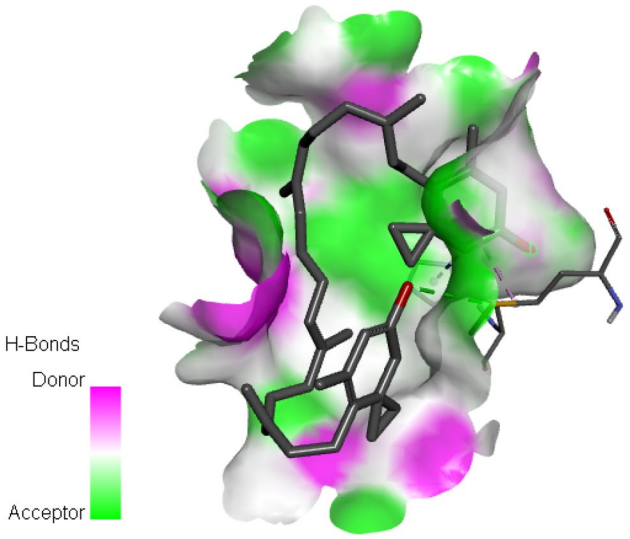

Fig. 5 presents the 3D interaction between the Lutein and the active sites of the protein

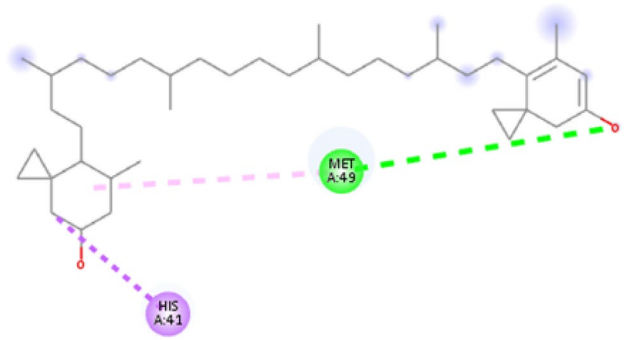

Fig. 6 2D protein–ligand interactions at the s-pike protein active site

Conclusions

In conclusion, a molecular docking study was performed, to predict the mechanism of action behind the polyphenolic compounds inhibition activity against COVID-19 virus. To prevent eye illnesses including cataracts and a condition that causes vision loss in elderly persons, lutein is frequently taken orally (age-related macular degeneration or AMD). There are several more disorders for which lutein is utilised, but no strong scientific evidence supports any of these other applications. The obtained results showed that Lutein (from green leafy vegetables such as spinach) has the highest affinity with the Spike protein of COVID-19 in comparison with the other polyphenolic molecules. This work highlights the potential of Lutein using a combined computational/approach. Despite showing moderate activities, the exploitation of Lutein as natural ingredients would help to increase the immunity against COVID-19 virus. In the future, protein components in COVID-19 virus can be studied and analysed for findings of medicine or vaccination.

Author contributions There is no authorship contribution.

Funding No funding is involved in this work.

Data availability Based on the request authors can provide.

Declarations

Conflict of interest Conflict of interest is not applicable in this work.

Ethical approval No participation of humans takes place in this implementation process.

Human and Animal Rights No violation of Human and Animal Rights is involved.

References

Abdelsattar AS, Dawoud A, Helal MA (2021) Interaction of nanoparticles with biological macromolecules: a review of molecular docking studies. Nanotoxicology 15(1):66–95

Achraf A, Hamdi C, Turki M, Abdelkarim O, Ayadi F, Hoekelmann A, Souissi N (2018) Natural pomegranate juice reduces inflammation, muscle damage and increase platelets blood levels in active healthy Tunisian aged men. Alexandria J Med 54(1):45–48

Alihosseini F (2016) "Plant-based compounds for antimicrobial textiles, in antimicrobial textiles" Elsevier. 155–195

E. Balboni, et al. (2022) "Zinc and selenium supplementation in COVID-19 prevention and treatment: a systematic review of the experimental studies". J Trace Elements Med Bio 126956

Bimonte S et al (2019) Epigallocatechin-3-gallate in the prevention and treatment of hepatocellular carcinoma: experimental findings and translational perspectives. Drug Des Dev Ther 13:611

Chai SC, Kristina D, Zugui Z, Longying Z , Kenneth FK (2019) Effects of tart cherry Juice on Biomarkers ofInflammation and oxidative stress in Older Adults. Nutrients 11: 228

Chen D, Oezguen N, Urvil P, Ferguson C, Dann SM, Savidge TC (2016) Regulation of protein-ligand binding affinity Byhydrogen bond pairing. Sci Adv 2(3):e1501240

Cory H, Passarelli S, Szeto J, Tamez M, Mattei J (2018) The role of polyphenols in human health and food systems: a mini-review. Front Nutr 5(87):1–9

C Costa et al (2017) Current evidence on the effect of dietary polyphenols intake on chronic diseases. Food Chem Toxicol 110:286–299

S. Das, S. Sarmah, S. Lyndem, A Singha Roy (2021) "An investigation into the identification of potential inhibitors of SARS-CoV-2 main protease using molecular docking study".J.Biomol. Struct. Dyn. 39 (9) 3347–3357

Deghady AM, Hussein RK, Alhamzani AG, Mera A (2021) Density functional theory and molecular docking investigations of the chemical and antibacterial activities for 1-(4-Hydroxyphenyl)-3-phenylprop-2-en-1-one. Molecules 26:3631

Dennington R, Keith T, Millam J (2009) GaussView, Version 5.0.8.: Semichem Inc., Shawnee Mission KS

Dilshad R, Ahmad S, Aati HY, Al-qahtani JH, Sherif AE, Hussain M, Ahmed M (2022) Phytochemical profiling, in vitro biological

activities, and in-silico molecular docking studies of Typha domingensis. Arab J Chem 15(10):104133
Donthu N, Gustafsson A (2020) Effects of COVID-19 on business and research. J Business Res 117:284–289
GiusiBriguglio, Chiara Costa, Manuela Pollicino, Federica Giambò ,Stefania Catania, ConcettinaFenga. (2020)"Polyphenols in cancer prevention: New insights (Review) .International JournalofFunctionalNutrition 1 (2)
Gössling S, Scott D, Hall CM (2020) Pandemics, tourism and global change: a rapid assessment of COVID-19. J Sustain Tour 29(1):1–20
Hilbert M (2016) Big data for development: a review of promises and challenges. Development Policy Rev 34(1):135–174
Hsu S. (2015) "Compounds derived from epigallocatechin-3-gallate (EGCG) as a novel approach to the prevention of viral infections". Inflammation and allergy-drug targets (Formerly current drug targets-inflammation and allergy) (Discontinued) 14 (1) 13–18
Huey R, Morris GM, Forli S (2012) Using AutoDock 4 and AutoDock vina with AutoDockTools: a tutorial. Scripps Res Institute Molecular Graphics Lab 10550:92037
Islam R, Parves MR, Paul AS, Uddin N, Rahman MS, Mamun AA, Hossain MN, Ali MA, Halim MA (2021) A molecular modeling approach to identify effective antiviral phytochemicals against the main protease of SARS-CoV-2. J Biomol Struct Dyn 39(9):3213–3224
Kh. Kafi Dh. Ayyash A. N, .Mohammed A. S, (2019) "Theoretical Study of Structural Properties and Energies of a 2-Aminophenol –Vanillin Molecule" .IOP Conf. Series: J Phy: Conf. Series 1178 012007
Le TT et al (2020) The COVID-19 vaccine development landscape. Nat Rev Drug Discov 19(5):305–306
Machhi J et al (2020) The natural history, pathobiology, and clinical manifestations of SARS-CoV-2 infections. J Neuroimmune Pharmacol 15(3):359–386
Pham Q.V et al. (2020) "Artificial intelligence (AI) and big data for coronavirus (COVID-19) pandemic: A survey on the state-of-the-arts". IEEE access 8 130820
PhilippeBuchy, SibelAscioglu, YvesBuisson, SanjoyDatta, MichaelNissen, Paul AnantharajahTambyah, SirendaVong (2020) "Impact of vaccines on antimicrobial resistance". International Journal of Infectious Diseases 90 (3) 188–196
Reich P, Elward A (2022) Infection Prevention during the coronavirus disease 2019 pandemic. Infectious Disease Clinics North Am 36(1):15–37
Sathish M. , Meenakshi G. , Xavier S. , Sebastian S. , Sathana V., (2017) "Vibrational spectroscopic and molecular docking studies on N-Carbobenzoxy-L-2-phenylglycine by density functional theory method". Asian J. Chem. 29 (2) 242–256
Shelley JC et al (2007) Epik: a software program for pK a prediction and protonation state generation for drug-like molecules. J Comput Aided Mol Des 21(12):681–691
Sherman W, Beard HS, Farid R (2006) Use of an induced fit receptor structure in virtual screening. Chem Biol Drug Des 67(1):83–84
D. Studio, (2008) "Discovery Studio". Accelrys [2.1]
Thuy BTP et al (2020) Investigation into SARS-CoV-2 resistance of compounds in garlic essential oil. ACS Omega 5(14):8312–8320
Tresanco MS et al (2020) AMDock: a versatile graphical tool for assisting molecular docking with Autodock Vina and Autodock4. Biol Direct 15(1):1–12
M.M. Vuolo, V.S. Lima, and M.r.R.M. Junior, (2019) "Phenolic compounds: Structure, classification, and antioxidant power, in Bioactive compounds", Elsevier. 33–50